

Article

Insights into the Role of Pt Promoter in Co/TiO₂ Catalysts for CO Hydrogenation

Changsong Hu ^{1,2}, Chengwu Qiu ¹, Wenli Zhang ^{1,2}, Jinliang Song ^{1,2}, Qingwei Meng ^{1,2,*}, Qingchun Yuan ^{3,*} and Tiejun Wang ^{1,2}

¹ School of Chemical Engineering and Light Industry, Guangdong University of Technology, Guangzhou 510006, China

² Guangdong Provincial Laboratory of Chemistry and Fine Chemical Engineering Jieyang Center, Jieyang 515200, China

³ Energy and Bioproducts Research Institute, College of Engineering and Physical Sciences, Aston University, Birmingham B4 7ET, UK

* Correspondence: qwmeng@gdut.edu.cn (Q.M.); q.yuan@aston.ac.uk (Q.Y.)

Abstract: Platinum is widely used as a reduction promoter in transition metal heterogeneous catalysts, while its effects on the catalyst's properties and CO hydrogenation behavior remain unclear. In this study, an improvement in the reducibility of platinum-promoted catalysts is observed. Notably, platinum suppresses the aggregation of cobalt nanoparticles (CoNPs) during catalyst preparation, as evidenced by STEM/TEM and XRD analyses, which reveal the presence of smaller CoNPs and weakened cobalt diffraction in platinum-promoted catalysts. In addition, platinum also promotes the formation of more active hexagonal close-packed (hcp) cobalt but inhibits metal-support interaction (MSI). Therefore, the cobalt-time yield (CTY) for CO hydrogenation in the promoted catalyst is strongly improved, and, furthermore, its intrinsic activity (turnover frequency, TOF) is also slightly increased. However, the product distribution seems unchanged except for the CO₂ for the platinum-promoted catalysts.

Keywords: Co/TiO₂; platinum promoter; CO hydrogenation; reducibility



Citation: Hu, C.; Qiu, C.; Zhang, W.; Song, J.; Meng, Q.; Yuan, Q.; Wang, T. Insights into the Role of Pt Promoter in Co/TiO₂ Catalysts for CO Hydrogenation. *Catalysts* **2024**, *14*, 922. <https://doi.org/10.3390/catal14120922>

Academic Editor: Maria A. Goula

Received: 1 November 2024

Revised: 3 December 2024

Accepted: 11 December 2024

Published: 14 December 2024



Copyright: © 2024 by the authors. Licensee MDPI, Basel, Switzerland. This article is an open access article distributed under the terms and conditions of the Creative Commons Attribution (CC BY) license (<https://creativecommons.org/licenses/by/4.0/>).

1. Introduction

Oxide, including SiO₂, TiO₂, Al₂O₃, CeO₂, and zeolite, is the typical support in heterogeneous catalysts [1–3] and is primarily used as a medium to deliver the active component. Among those, TiO₂-supported CoNPs are a widely reported heterogeneous catalyst [1,4–6]. TiO₂ as a support is often used to study the strong metal-support interaction (SMSI) due to the reducible nature of TiO₂. The active metal phase is often blocked by the reduced TiO_{2-x} easily formed during reduction and is, therefore, inimical to the adsorbability and catalytic performance of the catalyst [5,6]. Furthermore, this SMSI shows a dependency on the TiO₂ polymorph and the supported metal nanoparticle size, with anatase (vs. rutile) and a large nanoparticle size (3–13 nm) being more susceptible to this phenomenon [7–10]. In addition, reducibility is an additional concern for the TiO₂-supported transition metal catalysts. This originates in the formation of metal-support compounds (MSC) between the transition metal and the support, e.g., the non-reducible cobalt titanate in a Co/TiO₂ catalyst [11,12], leading to a loss of active metal for catalytic reactions. Such titanate compound formation, undesirably, can be exacerbated by close contact between the transition metal and TiO₂, for example, the spreading of cobalt on the titania surface [13,14]. Fortunately, recent work showed that creating surface oxygen vacancies or removing surface oxygen atoms can significantly promote the reduction of supported cobalt oxides [15]. Also, the surface modification of the TiO₂ support is also reported to minimize the formation of MSC, where TiO₂ is coated with a third material such as carbon and SiO₂ [16].

Alternatively, another simple and effective way to improve the reducibility is confirmed to be the addition of small amounts of noble metals [17]. Noble metals such as platinum can easily dissociate adsorbed H_2 [18–21], which then spills over onto the active species like cobalt via TiO_2 to promote the reduction of cobalt oxide [22–25]. Beaumont et al. reported that smaller Pt nanoparticles (1.9 vs. 12 nm) with CoNPs nearby show a better promotional effect on cobalt oxide reduction [22]. As it can continuously remove surface oxygen under reaction conditions, the activity of CO_2 or CO hydrogenation can be strongly enhanced. Also, den Otter et al. found that Pt-promoted Co/ SiO_2 and CoNb/ SiO_2 can remarkably improve a catalyst's reducibility and the following Fischer–Tropsch synthesis (FTS) activities [26]. They also showed that the addition of platinum can change the product selectivity (depending on the reaction pressure) and decrease the CoNP size. At high pressure (20 bar), platinum addition decreases the C_{5+} selectivity, while at low pressure, the C_{5+} selectivity is improved. However, the effect of the platinum promoter on the supported cobalt nanoparticle size is still controversial. Zhang et al. reported that platinum has no significant effect on the size of Co_3O_4 nanoparticles in a carbon nanotube-supported catalyst but can improve the stability of the catalyst in FTS [27–31]. In contrast, Vosoughi et al. observed improved cobalt dispersion in a platinum-promoted cobalt mesoporous alumina catalyst, thus leading to improved active sites and stability of the catalysts for FTS [32]. The platinum promotional effect on metal dispersion was also occasionally observed by other researchers [25,33,34]. However, many researchers believe that metal dispersion is more influenced by the nature of the support, such as the pore structure and MSI [26,27,33], or by the catalyst preparation method [35]. As a promoter, platinum initially is designed to form, for example, a Pt–Co alloy [36]. However, cobalt and platinum tend to segregate, especially at high platinum loadings [37,38], which makes it complex to study the role of platinum. So, well-defined Co and Pt NPs with controllable size, interparticle distance, and core-shell structure were previously prepared for this task [22,23,39].

Herein, to further probe the effects of platinum addition on transition metal catalysts, we report a microemulsion coupled with a deposition method to prepare platinum-promoted and unpromoted Co/ TiO_2 catalysts. It is proposed that their nanoparticle sizes and the mixing of cobalt and platinum can be well controlled. Unexpectedly, despite using the same micelle solution, the different metal precursors (cobalt nitrate solution versus a cobalt/platinum nitrate solution of the same concentration) resulted in significant variations in the size distribution of the metal nanoparticles on the catalyst surface. Platinum can significantly maintain the nanoparticle size by preventing the aggregation of CoNPs ($Co(OH)_2$) during their deposition on TiO_2 . As platinum can also promote cobalt oxide reduction, CO hydrogenation activities in the promoted catalysts are significantly enhanced while the product yields are not affected. The desired hcp active phase of CoNPs is also surprisingly promoted to form CO_2 although with an unclear reason to date. Exceptionally, CO_2 formation is strongly boosted with over a 300% yield in platinum-promoted catalysts detected.

2. Results and Discussion

2.1. Improved Activities of CO Hydrogenation on Platinum-Promoted Catalysts

The CO hydrogenation activities of the catalysts (493 K, $H_2/CO = 10$, 1 bar) are shown in Figure 1. CO conversion on 5CoPt/15CoPt (30~35%) is observed to be roughly 2~3-fold higher than that on 5Co/15Co (10~17%) throughout the reaction time (Figure 1a). A similar activity gap between the platinum-promoted and unpromoted samples is also seen in Figure 1b, which is converted to CTY for each catalyst, i.e., >120 vs. ~50 $mmol_{CO}/g_{Co}^{-1}\cdot h^{-1}$ in 5CoPt/5Co or ~60 vs. ~30 $mmol_{CO}/g_{Co}^{-1}\cdot h^{-1}$ in 15CoPt/15Co. Interestingly, 5CoPt/5Co catalysts are more active than those high-loaded 15CoPt/15Co (~2-fold difference in CTY). The intrinsic activity, i.e., the TOF, for each catalyst is calculated in Figure 1c. The data clearly show that the TOF values for the platinum-promoted catalysts are slightly higher than those of the unpromoted catalysts under identical reaction conditions. Similarly, the catalysts with low cobalt loadings also show higher intrinsic activities. This means that platinum addition and TiO_2 support (i.e., MSI) have positive effects on the intrinsic

activities of Co/TiO₂ catalysts. The accompanying product distributions of 5Co/5CoPt and 15Co/15CoPt determined from MS profiles are given in Figures S1 and S2. The actual selectivities of CH₄/C₂/C₃/C₄/C₅ hydrocarbons and CO₂ are hardly obtained based on the MS data, but the relative MS intensities of hydrocarbons (to methane) are calculated to describe the product distribution (Figure 1d and Figure S3). Under the reaction conditions, CH₄ is the primary hydrocarbon (>80%) compared with other minimal products. Additionally, CO₂ production is notably higher with platinum-promoted catalysts compared to unpromoted catalysts. The CO₂ formation could derive from the water–gas shift reaction, the Boudouard reaction, or the carburization reaction [40]. However, which reaction leads to the CO₂ formation here is not clear, but it could partly be due to the high amount of surface oxygen vacancies and surface OH groups in the promoted catalysts [41,42].

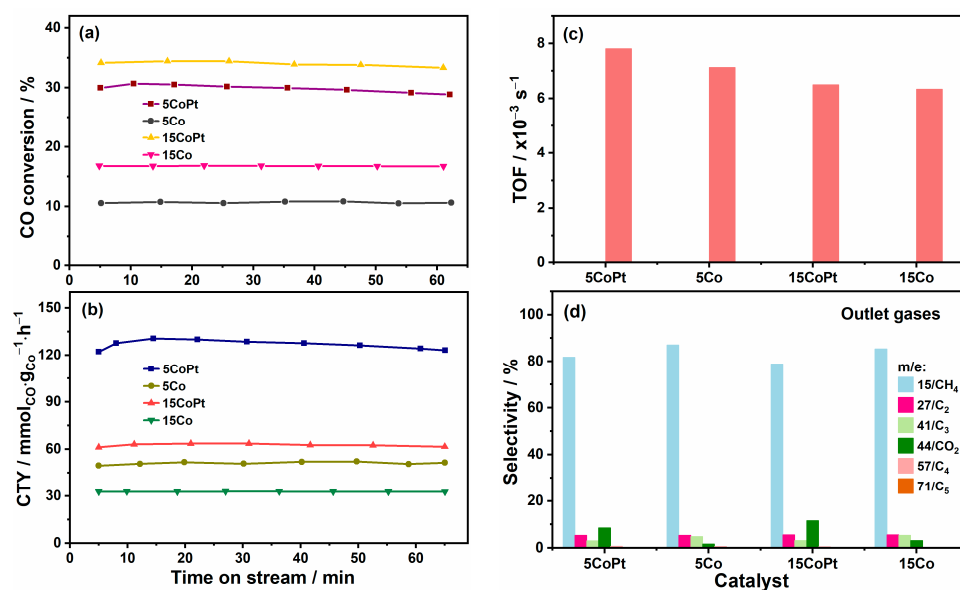


Figure 1. CO hydrogenation activity of the catalysts under conditions of 493 K, 1 bar, and H₂/CO = 10. (a) CO conversion; (b) Cobalt time yield (CTY) (corrected with corresponding DOR value); (c) TOF after reaction for 30 min; (d) Relative product distributions. The activities are strongly enhanced for the catalysts with the addition of platinum and a low cobalt loading.

2.2. Identifying Surface Properties, Nanoparticle Sizes, and Active Components of the Catalysts

To elucidate the reaction differences in those catalysts, we first measured the N₂ physical adsorption to determine their surface areas as well as their pore volumes and diameters (Table 1). It was found that catalysts with a platinum promoter and higher loading possess higher surface areas and larger pore structures. Since the same rutile support was used in all the catalysts, the above differences are attributed to the contribution of supported nanoparticles (i.e., their concentrations and nanostructures). From Figure 2, it is evident that the average CoNP size in 5Co (10.08 nm) is significantly larger than that in 5CoPt (5.25 nm). The catalysts at a higher cobalt loading also exhibit such size differences that the unpromoted 15Co catalyst yields larger CoNPs (13.34 nm) than the 15CoPt (7.68 nm) (Figure S4). Then, the XRD patterns for these samples (diffraction of Co(OH)₂ and Co⁰, Figure 3) further confirm the difference in the NP size and that catalysts with the promotion of platinum and a low cobalt loading show small and broad diffraction peaks both before and after H₂ reduction. However, for the samples 5Co/15Co, the reflections always appear narrower, which is indicative of larger crystallites (Figure 3). Interestingly, where a Scherrer analysis can be performed on reduced catalysts, there is a good correlation with the average particle size as determined from the STEM/TEM images (i.e., 16.26 nm of CoNPs for 15Co, 11.37 for 5Co, 10.56 for 15CoPt, and 6.08 nm for 5CoPt). The larger NP sizes in unpromoted catalysts are due to the aggregation of initial CoNPs during demulsification although we used the same micelle solution to prepare the catalysts, and particularly high cobalt loading exacerbates such aggregation. The FTIR

absorption (1384 cm^{-1}) in Figure S5 confirms such aggregation, as a stronger aggregation of NPs will lead to more nitrate compounds being encapsulated in the calcined samples [43]. Fortunately, those nitrate compounds can be decomposed or removed after reduction treatment since such nitrate absorption peaks disappear in the reduced catalysts (Figure S5). Additionally, for the platinum-promoted catalyst (e.g., 5CoPt), cobalt and platinum are not homogeneously mixed. Bare PtNPs, the Pt-core-Co-shell structure, and a Co–Pt alloy can be identified in the platinum-promoted catalyst (Figure 2c,d). The crystal phases of cobalt for the promoted and unpromoted catalysts are analyzed in Figures 2b,d and 3. For both of the catalysts, face-centered-cubic (fcc) cobalt would occupy the major phase from the FFT patterns in Figure 2b and the XRD patterns in Figure 3. However, for platinum-promoted catalysts, particularly 5CoPt, the hcp cobalt can be clearly observed in Figures 2d and 3. The reason for the formation of different cobalt crystal phases in the two types of catalysts is not clear. However, in previous studies, hcp cobalt was identified to exhibit higher intrinsically active CO hydrogenation than the fcc phase [44,45]. TiO_2 is partly reduced to Ti_2O_3 in both types of catalysts, as seen in Figure 2b,d. This Ti_2O_3 is not detected on the surface of CoNPs for 5CoPt (Figure 2c,d), but its FFT pattern is measured on the CoNP in 5Co (Figure 2b, region 2). As such, the SMSI is weakened in 5CoPt, which will promote the adsorbability and hydrogenation activity [5,6]. All of the above indicate that a high TOF or CTY can be present in platinum-promoted catalysts, corresponding to the reaction results in Figure 1 [45,46].

The H_2 -TPR profiles in Figure 4 illustrate the reducibility of the promoted and unpromoted catalysts. Compared with 5CoPt/15CoPt, the reduction of 5Co/15Co catalysts is strongly delayed with an observation of the H_2 consumption peaks extremely shifting to a high temperature. In 5Co, the peaks are attributed to the reduction of $\text{Co}(\text{OH})_2$ and Co_3O_4 to Co^0 and CoTiO_3 to Co^0 , respectively [11,47]. By increasing the cobalt loading to 15 wt. %, 15Co shows a different reduction behavior. First, there is a small double peak centered at 521 K, which was previously ascribed to the reduction of unsupported Co_3O_4 NPs [48,49], reflecting the aggregation of CoNPs in this sample. In fact, the aggregation (with a low extent) in 5Co is also evident with a small bump at around 500 K. Then, the later H_2 consumption peak in the 15Co sample (Figure 4) is centered at 654 K but with two shoulders at 626 and 726 K. These correspond to the overlapped reduction of $\text{Co}(\text{OH})_2/\text{Co}_3\text{O}_4 \rightarrow \text{Co}^0$. There is only minimal H_2 consumption after 726 K in this sample, indicating negligible cobalt–titania interaction or CoTiO_3 formation.

In contrast, 5CoPt/15CoPt catalysts are ready to reduce with almost all the H_2 consumption peaks observed at temperatures below 700 K, corresponding to PtO_2 and $\text{Co}(\text{OH})_2/\text{Co}_3\text{O}_4$ reduction to Pt^0 and Co^0 , respectively. This can be attributed to the strong promotional effect of Pt via H_2 spillover and that the dissociated H under the promotion of Pt migrates onto cobalt oxides to enforce their reduction [22–24]. Specifically, the reduction of 5CoPt seems more difficult than that of 15CoPt (e.g., the presence of a peak at 815 K in 5CoPt, Figure 4). It is proposed that highly dispersed PtNPs in the low-loading catalyst cannot accumulate enough H spillover onto cobalt oxides and promote their reduction. H_2 spillover seems irrelevant to physical or chemical contact between platinum and cobalt [24], but TiO_2 can significantly promote such a spillover effect [23]. Exceptionally, for the Pt-core-Co-shell structure, the promotional effect of the Pt-core is thought to be minimal since the Co-shell will isolate the Pt-core from initially contacting the H_2 . A reverse Co-core-Pt-shell structure was confirmed to be ineffective for CO hydrogenation as its active phase cobalt was encapsulated [22]. Smaller CoNPs in 5CoPt (Figure 2, Figure 3 and Figure S4) leading to a stronger cobalt–titania interaction can also have a negative effect on the reduction of CoNPs. Therefore, more cobalt titanate (CoTiO_3) species can be formed and present in 5CoPt and are known to be more difficult to reduce than cobalt oxides [11,47]. The 15CoPt sample should contain similar Co/Pt nanostructures, but its high loading will weaken the cobalt–titania interaction and enhance the H_2 spillover effect to promote the reduction. The degree of reduction (DOR) of the catalysts under reduction at 623 K with 10% H_2/N_2 for 3 h is 86.8% for 5CoPt, 69.1% for 5Co, 100.0% for 15CoPt, and 85.2% for 15Co, respectively, reflecting the strong promotional effect of Pt and the weak MSI in high-loaded samples.

The XPS spectra in Figures 5 and S6 show the element components and their chemical environments in both the 5Co and 5CoPt catalysts. In contrast to the observations in Figures 3 and 4, the Co^{2+} species as the main components in both cases (Figure 5a) are due to passivation before XPS measurements. However, more metal cobalt in the 5CoPt sample (15.2%) was still fitted out in comparison with 5Co (10.6%), indicating that more metal cobalt can be maintained in the 5CoPt sample. For Co^{2+} species, there are two types, i.e., Co^{2+} (I) and Co^{2+} (II), corresponding to CoO and CoTiO_3 , respectively [50,51]. From Figure 5a, the amount of CoTiO_3 in 5CoPt (37.4%) is significantly higher than that in 5Co (15.5%), implying a stronger MSI derived from the intimate contact between the cobalt and TiO_2 and the high dispersion of cobalt in the 5CoPt sample. This high dispersion of cobalt is also confirmed by more surface cobalt calculated from the XPS survey spectra (see Figure 5c). This seems to be a contradiction to the H_2 -TPR results shown in Figure 4, which indicate that platinum-promoted catalysts should have less cobalt titanate. In fact, the presence of more CoTiO_3 from the 5CoPt XPS Co 2p spectrum is largely due to the reoxidation of the reduced cobalt during passivation. Fortunately, CoTiO_3 is not largely present in the in situ reduced catalysts.

Table 1. Textural properties of the catalysts.

Catalyst	BET Surface Area ^a /m ² /g	BJH Pore Volume ^a /cm ³ /g	BJH Pore Diameter ^a /nm	CoNP Size ^b /nm	
				STEM/TEM	XRD
5Co	33.64	0.19	1.94	10.08/10.29	11.37
5CoPt	38.73	0.22	2.11	5.25/5.80	6.08
15Co	44.72	0.15	3.81	-/13.34	16.26
15CoPt	55.59	0.24	3.82	-/7.68	10.56

^a, measured from calcined catalysts; ^b, determined from reduced catalysts.

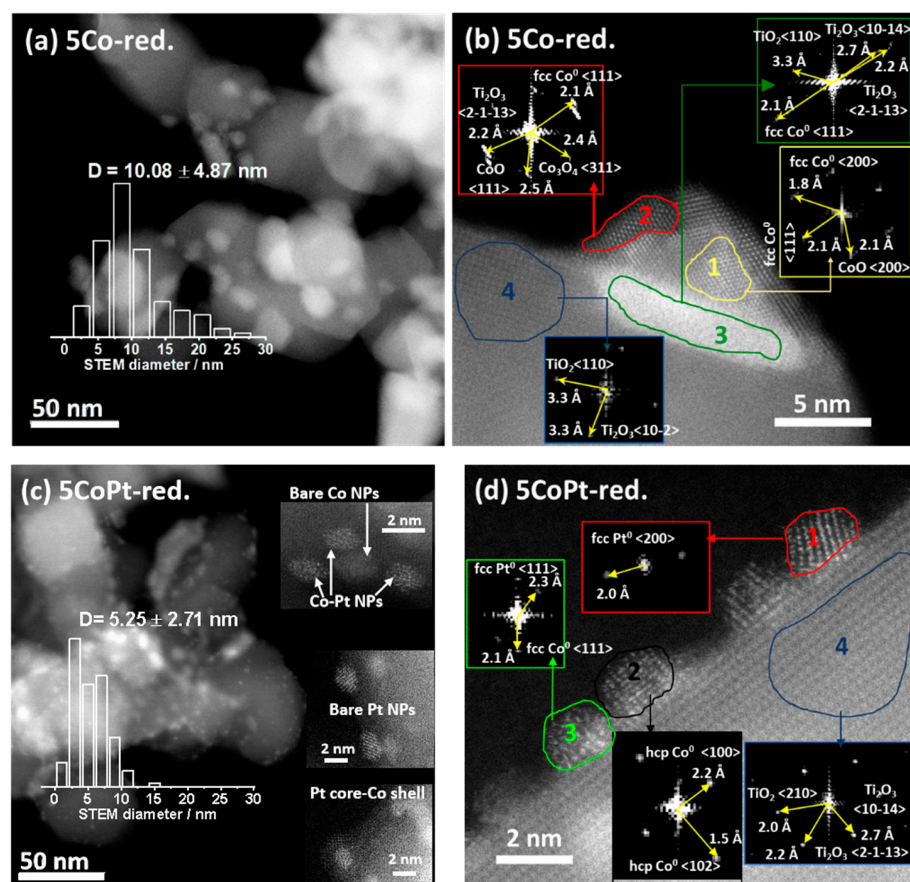


Figure 2. STEM images of reduced 5Co (a,b) and 5CoPt (c,d) catalysts. Small CoNPs (hcp and fcc crystals) without migration of Ti_2O_3 are seen in the platinum-promoted catalysts.

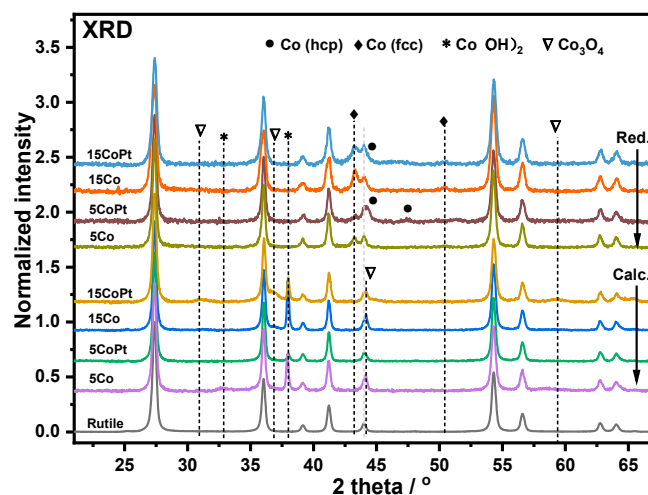


Figure 3. XRD patterns of calcined and reduced catalysts. Weak diffraction peaks of cobalt are found in the catalysts with platinum addition, meaning their smaller CoNPs. In addition, for unpromoted 5Co/15Co, only fcc cobalt can be detected, while for platinum-promoted 5CoPt/15CoPt, both fcc and hcp structures can be determined.

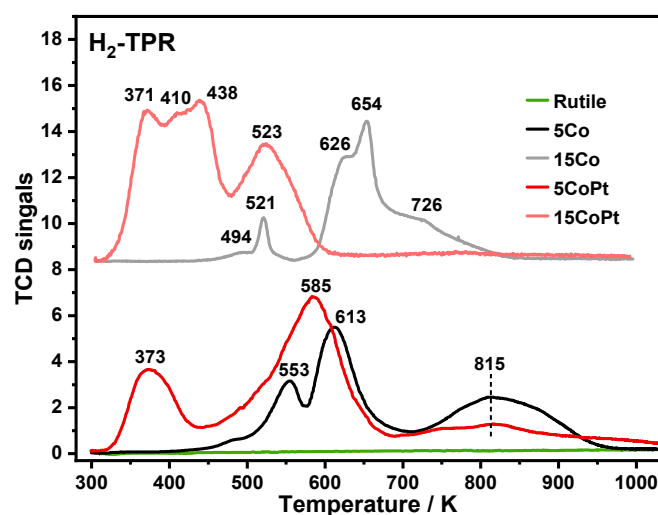


Figure 4. TPR profiles of the catalysts with and without platinum addition. H₂ consumption peaks of platinum-promoted catalysts significantly shifting to a low temperature indicates the promotional effect of platinum on the reducibility of the catalysts.

Figure 5b shows the XPS O 1s spectra of the 5Co and 5CoPt catalysts. The three deconvoluted peaks (529.7, 531.3, and 533.0 eV) refer to Ti-O (TiO₂), O_{vac}, and -OH, respectively. Generally, less surface Ti-O species (63.3%) but more Co-O/O_{vac} (28.3%) and -OH (8.4%) are seen in the 5CoPt catalyst than in the 5Co catalyst. This indicates the surface diversity of 5CoPt, which is due to the promotion of highly dispersed cobalt and platinum. However, the Ti species in both catalysts are roughly similar (Figure S6a); only minimal Ti³⁺ (<4%) was fitted out in the two catalysts. This is because rutile is the most thermally stable polymorph of TiO₂ and is difficult to reduce under the reduction conditions (623 K, 50% H₂/He) [9,52].

In situ, CO-DRIFTS spectra are shown in Figure 6 and Figure S7, where the strong linear adsorption peaks (2060/2065 cm⁻¹) of CO in the platinum-promoted 5CoPt sample are clearly observed, as reported in the literature [53–56]. This adsorption is persistent when elevating the temperature from 303 to 493 K, with only a 5 cm⁻¹ blue shift observed. Besides the linear adsorption, small bridged adsorption of CO at 1997 cm⁻¹ is also seen at 303 K; however, this adsorption disappears when the temperature is increased. In contrast, for 5Co, the adsorption peaks (at 303 K) are primarily below 2000 cm⁻¹, corresponding to the bridged adsorption of

CO, while the CO linear adsorption is minor (see 2049/2026 cm^{-1} in Figure 6). By increasing the temperature to 493 K, the adsorbed CO in the 5Co catalyst is largely removed with only a tiny peak at 1986 cm^{-1} observed. These findings suggest that the 5Co catalyst with fewer active sites shows weaker CO adsorption than the 5CoPt catalyst, which is in line with its low activity of CO hydrogenation (Figure 1). The less and bridged CO adsorption in 5Co would be partly due to its larger CoNP size (Figures 2 and 3) [36]. However, the bridged CO adsorption in those larger CoNPs can promote CO dissociation to shift the products majorly towards hydrocarbons, particularly long-chain hydrocarbons [57,58]. In comparison, the additional and linear CO adsorption in 5CoPt could be attributed to its much smaller CoNPs as well as the contribution of the platinum promoter. This CO adsorption mode is unsuitable for CO dissociation but could promote more CO_2 formation [59].

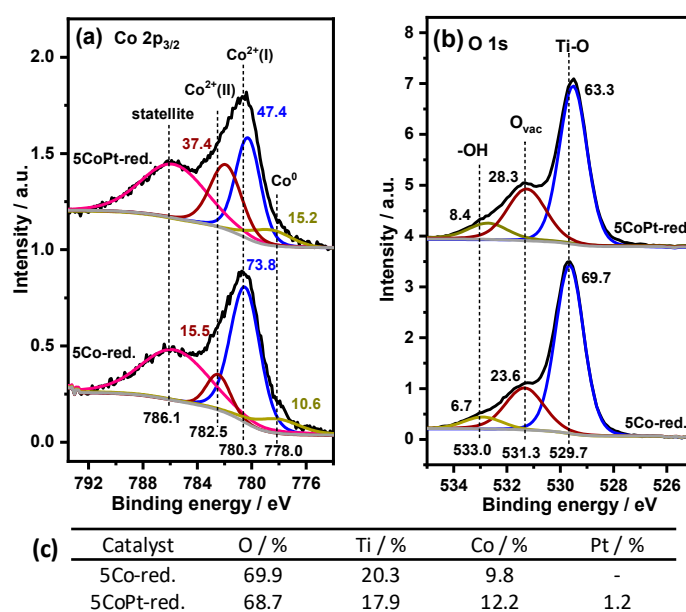


Figure 5. Fitted XPS $\text{Co } 2p_{3/2}$ (a) and $\text{O } 1s$ (b) spectra of reduced 5Co and 5CoPt catalysts. Both catalysts were reoxidized when exposed to air before the measurement. (c) Element components in each sample after H_2 reduction.

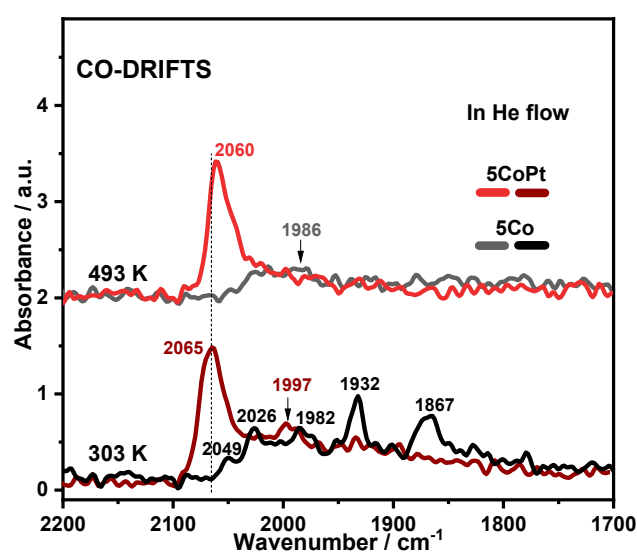


Figure 6. In situ CO-DRIFTS spectra of 5Co and 5CoPt catalysts after adsorbing CO for 30 min and then flushing He for 15 min. Strong linear adsorbed CO in 5CoPt catalyst cannot be desorbed under reaction temperature (493 K). In contrast, weak CO bridged adsorption on the 5Co catalyst is seen at 303 K and can be largely removed when elevating temperature to 493 K.

2.3. Rationalizing Reaction Performance with Catalyst's Properties

The activity differences between the two types of catalysts would be attributed to the active phase, the nanoparticle size, and the metal–support interaction. Generally, the active cobalt phase for CO hydrogenation is metallic cobalt, consisting of fcc and hcp crystal structures [44,45]. Therefore, the higher degree of reduction in the Pt-promoted catalysts can provide more metallic cobalt for CO hydrogenation, resulting in higher CO conversions. However, the discrepancies in the DOR (86.8 vs. 69.1% or 100.0 vs. 85.2%) cannot trigger those large activity differences between the promoted and unpromoted catalysts shown in Figure 1. In particular, the obvious differences still exist in the DOR corrected CTY and TOF in Figure 1b,c. However, the observed hcp phase in the platinum-promoted catalysts (Figures 2d and 3) can, indeed, improve the intrinsic activity of CO hydrogenation, and it is reported that the hcp cobalt in the FTS was around 5-fold more intrinsically active than the fcc phase [45]. This possibly illustrates the higher TOF values in the platinum-promoted catalysts. But the mechanism of forming more hcp cobalt in this promoted catalyst is unclear and the major phase is still fcc cobalt. The transition from fcc cobalt to hcp cobalt is attributed to the variances in the vibrational, magnetic, and electronic degrees of freedom within these lattice structures [60]. Notably, the absence of long-range magnetic interactions in fcc cobalt is crucial for the formation of hcp cobalt [61]. Consequently, it can be inferred that platinum may enhance the formation of hcp cobalt by perturbing long-range magnetic interactions [62–64].

Then, as seen in Figure 2, 3 and S4, the platinum-promoted catalysts possess smaller cobalt nanoparticle sizes. In this scenario, those two catalysts can provide more surface cobalt for a reaction. The fraction of surface cobalt is calculated to be 26.5% for 5CoPt, 12.7% for 5Co, 17.2% for 15CoPt, and 9.9% for 15Co [65]. Therefore, the activities (CTY) for the platinum-promoted catalysts (5–15CoPt) can reach a 2-fold higher value than the unpromoted ones (5–15Co), while that for low-loaded catalysts (5Co/5CoPt) can only be <1.5-fold higher than the high-loaded catalysts (15Co/15CoPt). The other factor here that can affect the CTY or further the TOF could be the nanoparticle size effect. There is a consensus that CoNPs below a critical size of 5–10 nm show low intrinsic activities (TOFs) in CO hydrogenation [65–67]. Our nanoparticle sizes in all the catalysts are higher than 5 nm, suggesting that the nanoparticle size effect here would not be significant [67]. However, the unpromoted catalysts would be still more intrinsically active than the promoted ones (see the major bridged CO adsorption in 5Co, Figure 6) due to their relatively larger nanoparticle sizes. This is a contradiction with the TOF values in Figure 1c, indicating the existence of other factors influencing the reaction differences.

From the reaction results in Figure 1, we know that catalysts with low loadings show higher activities, indicating the promotional effect of the MSI. The term MSI involves various nature changes in the catalysts like the components, morphology, charge transfer, etc. As shown in Figure 4, a catalyst with low loading or without a platinum promoter shows more H₂ consumption at a high temperature. This means that those catalysts possess more metal–support compounds, i.e., cobalt titanate in this case, which is an inactive phase for CO hydrogenation and can decrease the overall activity [68]. However, the CTY and TOF calculation has already excluded the effects of non-reducible cobalt titanate through correction with the DOR. Then, morphology changes of the cobalt nanoparticles will also strongly influence the activity. Here, the spreading of cobalt on the TiO₂ surface would not be significant from previous reports as the highest temperature here of only 623 K cannot lead to obvious spreading during reduction [13]. Since TiO₂ is a reducible support, the decoration of TiO_{2-x} (i.e., SMSI) is another morphology change we are discussing. To minimize the surface energy, the generated TiO_{2-x} can spontaneously migrate onto the supported metal nanoparticles and change their surface exposure and the following adsorbability [5,8,69,70]. However, rutile is the most thermally stable polymorph of TiO₂, and its reduction is considered to be weak [9] and can only decorate the peripheries of CoNPs, as seen in the STEM images in Figure 2b,d (particularly 5Co in Figure 2b). In addition, large nanoparticles (such as the largest 13.3 nm in 15Co) strongly decorated with

TiO_{2-x} were observed in previous work [10]. As a result, the CO adsorption in unpromoted catalysts is hindered, as shown in the DRIFTS spectra, and can be easily removed during heating (Figure 6 and S7). Of course, the bare platinum nanoparticles may also contribute to the linear CO adsorption in 5CoPt [41,71], but the amount would be small due to the extremely low Pt loading (atomic ratio Co/Pt = 10:1). Lastly, the charge effect here is not significant, although platinum as an electron donor can promote CO dissociation and the following CO hydrogenation [72]. The XPS binding energy shiftings of Co 2p, O 1s and Ti 2p are minimal, as seen in Figure 5 and Figure S6. Therefore, the higher activities of CO hydrogenation in the platinum-promoted catalysts are majorly due to their better reducibility and higher surface cobalt (i.e., small NP size) while partially resulting from the formation of hcp cobalt and a weak decoration effect.

3. Experimental Section

3.1. Catalyst Preparation

First, a tetraethylene glycol monododecyl surfactant (Sigma-Aldrich, Saint Louis, MO, USA) was dissolved in hexane (Sigma-Aldrich) at 303 K to form a reverse micelle solution. Then, a Co(NO₃)₂·6H₂O (Sigma-Aldrich, >98%) aqueous solution was added to acquire a pink liquid. Next, after adding pre-calcined pure rutile (773 K for 6 h), 28 wt. % NH₃ (aq) (Sigma-Aldrich) was dropwise added to generate solid Co(OH)₂ NPs, and then acetone (Sigma-Aldrich) was used to break the micelles and make the inner Co(OH)₂ NPs anchor onto the rutile support. Lastly, the acquired precipitation was filtered and washed 3–5 times with acetone before drying at 373 K for 12 h and calcining at 473 K for 5 h [73,74]. Those catalysts were designated as 5/15Co, indicating a composition with approximately 5/15 wt. % Co loading. For the platinum-promoted catalysts, denoted as 5/15CoPt, a mixture solution of cobalt nitrate and a platinum nitrate solution (Pt 15 % w/w, Alfa-Aesar, Ward Hill, MA, USA) were utilized, with a fixed Co/Pt atomic ratio of 10/1. The rest of the procedures were repeated as above for the 5/15Co catalysts. Sample reduction was achieved under the conditions of 50 vol. % H₂/He flow (20 mL/min) and 623 K for 3 h [75]. The reduced samples were protected either by passivation (1 vol. % O₂/He, 303 K, 50 mL/min, 30 min) or by the isolation of pure ethanol before further characterization.

3.2. Catalyst Characterization

Before measurements were obtained, each reduced or passivated sample was dispersed into ethanol using an ultrasonic bath (10 min) and then dropped onto a carbon film-coated copper TEM grid. After drying in air, TEM imaging was conducted using a JEOL JEM2100 TEM 200 kV instrument. HAADF-STEM was performed on a JEOL ARM200CF 200 kV microscope. The TEM/STEM images were analyzed using 1.52e ImageJ software [76,77], with the extraction of specific regions in Figure 2 for fast Fourier transformation (FFT). The NP size was averaged from the manual measurement of over 100 NPs.

XRD analysis was performed using a Rigaku Miniflex X-ray diffraction instrument (Cu K α 1, 45 kV, 2 θ 20–70°, step 0.01°, speed 0.2 s/°) with fixed divergence slits. Note that the measurement of the reduced samples was protected by the ethanol solvent and deposited a low noise Si background XRD holder.

A ChemBET Pulsar chemisorption analyzer (Anton Paar, Graz, Austria) was used to test the reducibility of the catalysts. Before performing H₂-TPR analysis, all the samples were pre-treated under pure He flow (50 mL/min) at 393 K for 30 min. Then, the H₂-TPR with a TCD detector was started at 303 K under 10 vol. % H₂/N₂ (50 mL/min) and, lastly, ramped to 1073 K (10 K/min). Specifically, an isothermal H₂-TPR at 623 K for 3 h (ramping procedure: 303 K→623 K (maintaining 3 h)→1073 K) was conducted to calculate the degree of reduction (DOR). The H₂ consumption ratios in the H₂-TPR profiles of \leq 623 K versus the total temperature range were the DOR of a corresponding catalyst.

Those pre-reduced samples with passivation were used to perform XPS analysis on a Thermo Fisher Scientific (Waltham, MA, USA) NEXSA spectrometer (Al X-ray source, 72 W, 400 microns). The samples were measured at room temperature and 10⁻⁹ mbar with

a charge neutralization mode and a pass energy of 50 eV (0.1 eV step size). The acquired data were analyzed by CasaXPS (version 2.3.19PR1.0) using a binding energy calibration of C 1s (284.8 eV) [78].

The transmission FTIR spectra were measured using a Nicolet (Madison, WI, USA) iS10 spectrometer (4 cm^{-1} spectral resolution). Before measurement, all the samples were dried at 373 K for 1 h, diluted with KBr powder, and pressed into 1 mm pellets. In situ CO adsorption (CO-DRIFTS) was carried out on an Agilent (Santa Clara, CA, USA) Cary 600 Series FTIR spectrometer. First, each catalyst was reduced under 50 vol. % H_2/He (30 mL/min) at 623 K for 3 h. Then, the catalyst was flushed with 10 vol. % CO/He at 303 K for 30 min before changing the gas to pure He (50 mL/min) to desorb the gaseous CO. DRIFTS spectra were recorded during CO and He flushing between 400 and 4000 cm^{-1} with a resolution of 4 cm^{-1} .

3.3. CO Hydrogenation

The activity of CO hydrogenation was tested on a CATLAB Microreactor (Hiden, Warrington, UK). In total, 150 mg of powder catalyst was first reduced in 50 vol. % H_2/He (20 mL/min) at 623 K for 3 h. Before switching to syngas ($\text{H}_2/\text{CO} = 10$, vol/vol) and ramping to 493 K, the catalyst needed to be cooled down to 423 K in the H_2/He flow. The hydrogenation reaction was performed at 1 atm. The outlet gases before and after the reaction were recorded using an equipped mass spectrometer (MS). The intensities of all the fragments, i.e., $m/e = 2$ (H_2), 15 (C_1), 18 (H_2O), 27 (C_2), 28 (CO), 41 (C_3), 44 (CO_2), 57 (C_4), and 71 (C_5), were calibrated using the inert standard gas He ($m/e = 4$).

4. Conclusions

Platinum as a promoter in Co/TiO₂ catalysts not only promotes the reduction of supported CoNPs but also prevents their aggregation in the catalysts. As a reduction promoter, platinum can significantly shift H₂-TPR profiles to a low temperature and enhance the reducibility of the catalysts. However, the extent of DOR enhancement by Pt addition cannot lead to large differences in the activity of CO hydrogenation. Since large differences were detected in the CoNP size (see STEM/TEM and XRD) and the surface fraction of cobalt between the promoted and unpromoted catalysts, the activity of CO hydrogenation was majorly attributed to those aspects. In addition, platinum promoted more hcp cobalt formation but weakened the MSI; thus, the CO adsorbability (see DRIFTS) and intrinsic activity for CO hydrogenation (TOF) were also slightly improved. Furthermore, these platinum-promoted catalysts can also promote CO₂ formation but cannot change the hydrocarbon yields. This work gives insights into the promotional roles of platinum in supported cobalt catalysts and guides us to design a catalyst with optimal dispersion and reducibility for catalytic reactions.

Supplementary Materials: The following supporting information can be downloaded at <https://www.mdpi.com/article/10.3390/catal14120922/s1>, Figure S1: MS intensities of hydrocarbons under H_2/CO volume ratio of 10 for 5Co/5CoPt catalysts; Figure S2: MS intensities of hydrocarbons under H_2/CO volume ratio of 10 for 15Co/15CoPt catalysts; Figure S3: Relative MS intensities of hydrocarbons to methane under H_2/CO volume ratio of 10; Figure S4: TEM images and corresponding histograms of reduced catalysts; Figure S5: FTIR spectra of the calcined and reduced catalysts; Figure S6: XPS Ti 2p (a) and Pt 4f (b) spectra of reduced 5Co and/or 5CoPt catalysts; Figure S7: CO-DRIFTS spectra of 5Co and 5CoPt catalysts, changing with He flushing time and temperature (the spectra records started at 303 K).

Author Contributions: Conceptualization, J.S., Q.M. and Q.Y.; methodology, C.H. and W.Z.; validation, C.Q. and W.Z.; formal analysis, C.H. and C.Q.; investigation, C.H. and W.Z.; resources, J.S., Q.Y. and T.W.; data curation, C.H. and C.Q.; writing—original draft preparation, C.H. and C.Q.; writing—review and editing, W.Z., Q.M. and Q.Y.; visualization, C.Q.; supervision, J.S., Q.Y. and T.W.; project administration, Q.M. and T.W.; funding acquisition, C.H. and Q.M. All authors have read and agreed to the published version of the manuscript.

Funding: This work was supported by the National Natural Science Foundation of China (52106235) and the National Key Research & Development Program of China (2023YFB4203604).

Data Availability Statement: The data are contained within the article and Supplementary Materials.

Conflicts of Interest: The authors declare no conflict of interest.

References

1. Storsæter, S.; Tøtdal, B.; Walmsley, J.C.; Tanem, B.S.; Holmen, A. Characterization of alumina-, silica-, and titania-supported cobalt Fischer-Tropsch catalysts. *J. Catal.* **2005**, *236*, 139–152. [[CrossRef](#)]
2. Gnanamani, M.K.; Ribeiro, M.C.; Ma, W.; Shafer, W.D.; Jacobs, G.; Graham, U.M.; Davis, B.H. Fischer-Tropsch synthesis: Metal-support interfacial contact governs oxygenates selectivity over CeO₂ supported Pt-Co catalysts. *Appl. Catal. A Gen.* **2011**, *393*, 17–23. [[CrossRef](#)]
3. Lee, J.H.; Bonte, W.; Corthals, S.; Krumeich, F.; Ruitenbeek, M.; van Bokhoven, J.A. Zeolite nanoreactor for investigating sintering effects of cobalt-catalyzed Fischer-Tropsch synthesis. *Ind. Eng. Chem. Res.* **2019**, *58*, 5140–5145. [[CrossRef](#)]
4. Voß, M.; Borgmann, D.; Wedler, G. Characterization of alumina, silica, and titania supported cobalt catalysts. *J. Catal.* **2002**, *212*, 10–21. [[CrossRef](#)]
5. Galván, M.C.Á.; Prats, A.E.P.; Campos-Martin, J.M.; Fierro, J.L. Direct evidence of the SMSI decoration effect: The case of Co/TiO₂ catalyst. *Chem. Commun.* **2011**, *47*, 7131–7133.
6. Hernández Mejía, C.; van Deelen, T.W.; de Jong, K.P. Activity enhancement of cobalt catalysts by tuning metal-support interactions. *Nat. Commun.* **2018**, *9*, 4459. [[CrossRef](#)]
7. van Deelen, T.W.; Hernández Mejía, C.; de Jong, K.P. Control of metal-support interactions in heterogeneous catalysts to enhance activity and selectivity. *Nat. Catal.* **2019**, *2*, 955–970. [[CrossRef](#)]
8. Tang, H.; Su, Y.; Zhang, B.; Lee, A.F.; Isaacs, M.A.; Wilson, K.; Li, L.; Ren, Y.; Huang, J.; Haruta, M. Classical strong metal-support interactions between gold nanoparticles and titanium dioxide. *Sci. Adv.* **2017**, *3*, e1700231. [[CrossRef](#)]
9. Bertella, F.; Concepción, P.; Martínez, A. TiO₂ polymorph dependent SMSI effect in Co-Ru/TiO₂ catalysts and its relevance to Fischer-Tropsch synthesis. *Catal. Today* **2017**, *289*, 181–191. [[CrossRef](#)]
10. Du, X.; Huang, Y.; Pan, X.; Han, B.; Su, Y.; Jiang, Q.; Li, M.; Tang, H.; Li, G.; Qiao, B. Size-dependent strong metal-support interaction in TiO₂ supported Au nanocatalysts. *Nat. Commun.* **2020**, *11*, 5811. [[CrossRef](#)]
11. Jongsomjit, B.; Sakdamnusun, C.; Goodwin, J.G.; Praserthdam, P. Co-support compound formation in titania-supported cobalt catalyst. *Catal. Lett.* **2004**, *94*, 209–215. [[CrossRef](#)]
12. Wolf, M.; Gibson, E.K.; Olivier, E.J.; Neethling, J.H.; Catlow, C.R.A.; Fischer, N.; Claeys, M. Water-induced formation of cobalt-support compounds under simulated high conversion Fischer-Tropsch environment. *ACS Catal.* **2019**, *9*, 4902–4918. [[CrossRef](#)]
13. Qiu, C.; Odarchenko, Y.; Meng, Q.; Cong, P.; Schoen, M.A.; Kleibert, A.; Forrest, T.; Beale, A.M. Direct observation of the evolving metal-support interaction of individual cobalt nanoparticles at the titania and silica interface. *Chem. Sci.* **2020**, *11*, 13060–13070. [[CrossRef](#)]
14. Cats, K.; Andrews, J.; Stéphan, O.; March, K.; Karunakaran, C.; Meirer, F.; De Groot, F.; Weckhuysen, B. Active phase distribution changes within a catalyst particle during Fischer-Tropsch synthesis as revealed by multi-scale microscopy. *Catal. Sci. Technol.* **2016**, *6*, 4438–4449. [[CrossRef](#)]
15. Qiu, C.; Odarchenko, Y.; Meng, Q.; Xu, S.; Lezcano-Gonzalez, I.; Olalde-Velasco, P.; Maccherozzi, F.; Zanetti-Domingues, L.; Martin-Fernandez, M.; Beale, A.M. Resolving the effect of oxygen vacancies on Co nanostructures using soft XAS/X-PEEM. *ACS Catal.* **2022**, *12*, 9125–9134. [[CrossRef](#)] [[PubMed](#)]
16. Liu, C.; He, Y.; Wei, L.; Zhao, Y.; Zhang, Y.; Zhao, F.; Lyu, S.; Chen, S.; Hong, J.; Li, J. Effect of TiO₂ surface engineering on the performance of cobalt-based catalysts for Fischer-Tropsch synthesis. *Ind. Eng. Chem. Res.* **2018**, *58*, 1095–1104. [[CrossRef](#)]
17. Eschemann, T.O.; Oenema, J.; de Jong, K.P. Effects of noble metal promotion for Co/TiO₂ Fischer-Tropsch catalysts. *Catal. Today* **2016**, *261*, 60–66. [[CrossRef](#)]
18. Yang, J.; Qi, Y.; Zhu, J.; Zhu, Y.-A.; Chen, D.; Holmen, A. Reaction mechanism of CO activation and methane formation on Co Fischer-Tropsch catalyst: A combined DFT, transient, and steady-state kinetic modeling. *J. Catal.* **2013**, *308*, 37–49. [[CrossRef](#)]
19. Chen, W.; Zijlstra, B.; Pilot, I.A.; Pestman, R.; Hensen, E.J. Mechanism of carbon monoxide dissociation on a cobalt Fischer-Tropsch catalyst. *ChemCatChem* **2018**, *10*, 136–140. [[CrossRef](#)]
20. Vasiliades, M.A.; Govender, N.S.; Govender, A.; Crous, R.; Moodley, D.; Botha, T.; Efstathiou, A.M. The effect of H₂ pressure on the carbon path of methanation reaction on Co/γ-Al₂O₃: Transient isotopic and operando methodology studies. *ACS Catal.* **2022**, *12*, 15110–15129. [[CrossRef](#)]
21. van Helden, P.; van den Berg, J.-A.; Weststrate, C.J. Hydrogen adsorption on Co surfaces: A density functional theory and temperature programmed desorption study. *ACS Catal.* **2012**, *2*, 1097–1107. [[CrossRef](#)]
22. Beaumont, S.K.; Alayoglu, S.; Specht, C.; Michalak, W.D.; Pushkarev, V.V.; Guo, J.; Kruse, N.; Somorjai, G.A. Combining in situ NEXAFS spectroscopy and CO₂ methanation kinetics to study Pt and Co nanoparticle catalysts reveals key insights into the role of platinum in promoted cobalt catalysis. *J. Am. Chem. Soc.* **2014**, *136*, 9898–9901. [[CrossRef](#)]

23. Karim, W.; Spreafico, C.; Kleibert, A.; Gobrecht, J.; VandeVondele, J.; Ekinci, Y.; van Bokhoven, J.A. Catalyst support effects on hydrogen spillover. *Nature* **2017**, *541*, 68–71. [[CrossRef](#)] [[PubMed](#)]
24. Nabaho, D.; Niemantsverdriet, J.H.; Claeys, M.; van Steen, E. Hydrogen spillover in the Fischer-Tropsch synthesis: An analysis of platinum as a promoter for cobalt-alumina catalysts. *Catal. Today* **2016**, *261*, 17–27. [[CrossRef](#)]
25. Jia, R.; Yu, F.; Lin, T.; An, Y.; Gong, K.; Zhong, L. Effects of noble metals on a Co₂C-based supported catalyst for Fischer-Tropsch to olefins. *Ind. Eng. Chem. Res.* **2022**, *61*, 4824–4831. [[CrossRef](#)]
26. Den Otter, J.H.; Nijveld, S.R.; De Jong, K.P. Synergistic promotion of Co/SiO₂ Fischer-Tropsch catalysts by niobia and platinum. *ACS Catal.* **2016**, *6*, 1616–1623. [[CrossRef](#)]
27. Zhang, H.; Chu, W.; Zou, C.; Huang, Z.; Ye, Z.; Zhu, L. Promotion effects of platinum and ruthenium on carbon nanotube supported cobalt catalysts for Fischer-Tropsch synthesis. *Catal. Lett.* **2011**, *141*, 438–444. [[CrossRef](#)]
28. Bezemer, G.L.; Bitter, J.H.; Kuipers, H.P.; Oosterbeek, H.; Holewijn, J.E.; Xu, X.; Kapteijn, F.; Van Dillen, A.J.; de Jong, K.P. Cobalt particle size effects in the Fischer-Tropsch reaction studied with carbon nanofiber supported catalysts. *J. Am. Chem. Soc.* **2006**, *128*, 3956–3964. [[CrossRef](#)] [[PubMed](#)]
29. Bezemer, G.L.; Radstake, P.; Koot, V.; Van Dillen, A.; Geus, J.; De Jong, K. Preparation of Fischer-Tropsch cobalt catalysts supported on carbon nanofibers and silica using homogeneous deposition-precipitation. *J. Catal.* **2006**, *237*, 291–302. [[CrossRef](#)]
30. Vasiliades, M.; Kalamaras, C.; Govender, N.; Govender, A.; Efstathiou, A.M. The effect of preparation route of commercial Co/ γ -Al₂O₃ catalyst on important Fischer-Tropsch kinetic parameters studied by SSITKA and CO-DRIFTS transient hydrogenation techniques. *J. Catal.* **2019**, *379*, 60–77. [[CrossRef](#)]
31. Fu, T.; Li, Z. Review of recent development in Co-based catalysts supported on carbon materials for Fischer-Tropsch synthesis. *Chem. Eng. Sci.* **2015**, *135*, 3–20. [[CrossRef](#)]
32. Vosoughi, V.; Dalai, A.K.; Abatzoglou, N.; Hu, Y. Performances of promoted cobalt catalysts supported on mesoporous alumina for Fischer-Tropsch synthesis. *Appl. Catal. A Gen.* **2017**, *547*, 155–163. [[CrossRef](#)]
33. Chu, W.; Chernavskii, P.A.; Gengembre, L.; Pankina, G.A.; Fongarland, P.; Khodakov, A.Y. Cobalt species in promoted cobalt alumina-supported Fischer-Tropsch catalysts. *J. Catal.* **2007**, *252*, 215–230. [[CrossRef](#)]
34. Mehrbod, M.; Martinelli, M.; Martino, A.G.; Cronauer, D.C.; Kropf, A.J.; Marshall, C.L.; Jacobs, G. Fischer-Tropsch synthesis: Direct cobalt nitrate reduction of promoted Co/TiO₂ catalysts. *Fuel* **2019**, *245*, 488–504. [[CrossRef](#)]
35. Cook, K.M.; Perez, H.D.; Bartholomew, C.H.; Hecker, W.C. Effect of promoter deposition order on platinum-, ruthenium-, or rhenium-promoted cobalt Fischer-Tropsch catalysts. *Appl. Catal. A Gen.* **2014**, *482*, 275–286. [[CrossRef](#)]
36. Tsubaki, N.; Sun, S.; Fujimoto, K. Different functions of the noble metals added to cobalt catalysts for Fischer-Tropsch synthesis. *J. Catal.* **2001**, *199*, 236–246. [[CrossRef](#)]
37. Weststrate, C.; Saib, A.; Niemantsverdriet, J. Promoter segregation in Pt and Ru promoted cobalt model catalysts during oxidation-reduction treatments. *Catal. Today* **2013**, *215*, 2–7. [[CrossRef](#)]
38. Pirola, C.; Scavini, M.; Galli, F.; Vitali, S.; Comazzi, A.; Manenti, F.; Ghigna, P. Fischer-Tropsch synthesis: EXAFS study of Ru and Pt bimetallic Co based catalysts. *Fuel* **2014**, *132*, 62–70. [[CrossRef](#)]
39. Beaumont, S.K.; Alayoglu, S.; Specht, C.; Kruse, N.; Somorjai, G.A. A nanoscale demonstration of hydrogen atom spillover and surface diffusion across silica using the kinetics of CO₂ methanation catalyzed on spatially separate Pt and Co nanoparticles. *Nano Lett.* **2014**, *14*, 4792–4796. [[CrossRef](#)] [[PubMed](#)]
40. Chakrabarti, D.; de Klerk, A.; Prasad, V.; Gnanamani, M.K.; Shafer, W.D.; Jacobs, G.; Sparks, D.E.; Davis, B.H. Conversion of CO₂ over a Co-based Fischer-Tropsch catalyst. *Ind. Eng. Chem. Res.* **2015**, *54*, 1189–1196. [[CrossRef](#)]
41. Jacobs, G.; Graham, U.M.; Chenu, E.; Patterson, P.M.; Dozier, A.; Davis, B.H. Low-temperature water-gas shift: Impact of Pt promoter loading on the partial reduction of ceria and consequences for catalyst design. *J. Catal.* **2005**, *229*, 499–512. [[CrossRef](#)]
42. Xu, M.; Yao, S.; Rao, D.; Niu, Y.; Liu, N.; Peng, M.; Zhai, P.; Man, Y.; Zheng, L.; Wang, B. Insights into interfacial synergistic catalysis over Ni@TiO_{2-x} catalyst toward water-gas shift reaction. *J. Am. Chem. Soc.* **2018**, *140*, 11241–11251. [[CrossRef](#)] [[PubMed](#)]
43. Xiao, B.; Zhu, W.; Li, Z.; Zhu, J.; Zhu, X.; Pezzotti, G. Tailoring morphology of cobalt-nickel layered double hydroxide via different surfactants for high-performance supercapacitor. *R. Soc. Open Sci.* **2018**, *5*, 180867. [[CrossRef](#)] [[PubMed](#)]
44. Liu, J.X.; Su, H.Y.; Sun, D.P.; Zhang, B.Y.; Li, W.X. Crystallographic dependence of CO activation on cobalt catalysts: HCP versus FCC. *J. Am. Chem. Soc.* **2013**, *135*, 16284–16287. [[CrossRef](#)]
45. Lyu, S.; Wang, L.; Zhang, J.; Liu, C.; Sun, J.; Peng, B.; Wang, Y.; Rappé, K.G.; Zhang, Y.; Li, J. Role of active phase in Fischer-Tropsch synthesis: Experimental evidence of CO activation over single-phase cobalt catalysts. *ACS Catal.* **2018**, *8*, 7787–7798. [[CrossRef](#)]
46. Gnanamani, M.K.; Jacobs, G.; Shafer, W.D.; Davis, B.H. Fischer-Tropsch synthesis: Activity of metallic phases of cobalt supported on silica. *Catal. Today* **2013**, *215*, 13–17. [[CrossRef](#)]
47. Riva, R.; Miessner, H.; Vitali, R.; Del Piero, G. Metal-support interaction in Co/SiO₂ and Co/TiO₂. *Appl. Catal. A Gen.* **2000**, *196*, 111–123. [[CrossRef](#)]
48. Zhang, Y.; Wei, D.; Hammache, S.; Goodwin Jr, J.G. Effect of water vapor on the reduction of Ru-promoted Co/Al₂O₃. *J. Catal.* **1999**, *188*, 281–290. [[CrossRef](#)]
49. Kim, D.S.; Kim, Y.H.; Yie, J.E.; Park, E.D. The effect of cobalt precursors on NO oxidation over supported cobalt oxide catalysts. *Korean J. Chem. Eng.* **2010**, *27*, 822–827. [[CrossRef](#)]

50. Huang, W.; Zuo, Z.; Han, P.; Li, Z.; Zhao, T. XPS and XRD investigation of Co/Pd/TiO₂ catalysts by different preparation methods. *J. Electron. Spectrosc. Relat. Phenom.* **2009**, *173*, 88–95. [[CrossRef](#)]
51. Jacobs, G.; Chaney, J.A.; Patterson, P.M.; Das, T.K.; Maillot, J.C.; Davis, B.H. Fischer-Tropsch synthesis: Study of the promotion of Pt on the reduction property of Co/Al₂O₃ catalysts by in situ EXAFS of Co K and Pt L_{III} edges and XPS. *J. Synchrotron Radiat.* **2004**, *11*, 414–422. [[CrossRef](#)]
52. Bagheri, S.; Muhd Julkapli, N.; Bee Abd Hamid, S. Titanium dioxide as a catalyst support in heterogeneous catalysis. *Sci. World J.* **2014**, *2014*, 727496. [[CrossRef](#)]
53. Chen, W.; Pestman, R.; Zijlstra, B.; Filot, I.A.; Hensen, E.J. Mechanism of cobalt-catalyzed CO hydrogenation: 1. Methanation. *ACS Catal.* **2017**, *7*, 8050–8060. [[CrossRef](#)] [[PubMed](#)]
54. Chen, W.; Filot, I.A.; Pestman, R.; Hensen, E.J. Mechanism of cobalt-catalyzed CO hydrogenation: 2. Fischer-Tropsch synthesis. *ACS Catal.* **2017**, *7*, 8061–8071. [[CrossRef](#)] [[PubMed](#)]
55. Jamaati, M.; Torkashvand, M.; Sarabadani Tafreshi, S.; de Leeuw, N.H. A review of theoretical studies on carbon monoxide hydrogenation via Fischer-Tropsch synthesis over transition metals. *Molecules* **2023**, *28*, 6525. [[CrossRef](#)] [[PubMed](#)]
56. Vasiliades, M.A.; Kyprianou, K.K.; Govender, N.S.; Govender, A.; Crous, R.; Moodley, D.; Efstathiou, A.M. The effect of CO partial pressure on important kinetic parameters of methanation reaction on Co-based FTS catalyst studied by SSITKA-MS and operando DRIFTS-MS techniques. *Catalysts* **2020**, *10*, 583. [[CrossRef](#)]
57. Tuxen, A.; Carencio, S.; Chintapalli, M.; Chuang, C.H.; Escudero, C.; Pach, E.; Jiang, P.; Borondics, F.; Beberwyck, B.; Alivisatos, A.P. Size-dependent dissociation of carbon monoxide on cobalt nanoparticles. *J. Am. Chem. Soc.* **2013**, *135*, 2273–2278. [[CrossRef](#)]
58. Munirathinam, R.; Pham Minh, D.; Nzihou, A. Effect of the support and its surface modifications in cobalt-based Fischer-Tropsch synthesis. *Ind. Eng. Chem. Res.* **2018**, *57*, 16137–16161. [[CrossRef](#)]
59. Krylova, A.Y. Products of the Fischer-Tropsch synthesis (a review). *Solid Fuel Chem.* **2014**, *48*, 22–35. [[CrossRef](#)]
60. Lizárraga, R.; Pan, F.; Bergqvist, L.; Holmström, E.; GerCSI, Z.; Vitos, L. First principles theory of the hcp-fcc phase transition in cobalt. *Sci. Rep.* **2017**, *7*, 3778. [[CrossRef](#)]
61. Katanin, A. Magnetic properties of a half metal from the paramagnetic phase: DFT+DMFT study of exchange interactions in CrO₂. *Phys. Rev. B* **2024**, *110*, 155115. [[CrossRef](#)]
62. Macheli, L.; Leteba, G.M.; Doyle, B.P.; Jewell, L.; van Steen, E. Modulating CO hydrogenation activity through silane functionalization of cobalt catalysts. *Appl. Catal. A Gen.* **2024**, *685*, 119874. [[CrossRef](#)]
63. Petit, C.; Rusponi, S.; Brune, H. Magnetic properties of cobalt and cobalt-platinum nanocrystals investigated by magneto-optical Kerr effect. *J. Appl. Phys.* **2004**, *95*, 4251–4260. [[CrossRef](#)]
64. Meier, F.; Lounis, S.; Wiebe, J.; Zhou, L.; Heers, S.; Mavropoulos, P.; Dederichs, P.H.; Blügel, S.; Wiesendanger, R. Spin polarization of platinum (111) induced by the proximity to cobalt nanostripes. *Phys. Rev. B* **2011**, *83*, 075407. [[CrossRef](#)]
65. van Helden, P.; Ciobîcă, I.M.; Coetzer, R.L. The size-dependent site composition of FCC cobalt nanocrystals. *Catal. Today* **2016**, *261*, 48–59. [[CrossRef](#)]
66. Agrawal, R.; Phatak, P.; Spanu, L. Effect of phase and size on surface sites in cobalt nanoparticles. *Catal. Today* **2018**, *312*, 174–180. [[CrossRef](#)]
67. Den Breejen, J.; Radstake, P.; Bezemer, G.; Bitter, J.; Frøseth, V.; Holmen, A.; de Jong, K.d. On the origin of the cobalt particle size effects in Fischer-Tropsch catalysis. *J. Am. Chem. Soc.* **2009**, *131*, 7197–7203. [[CrossRef](#)]
68. Wolf, M.; Fischer, N.; Claeys, M. Formation of metal-support compounds in cobalt-based Fischer-Tropsch synthesis: A review. *Chem Catal.* **2021**, *1*, 1014–1041. [[CrossRef](#)]
69. Tauster, S.; Fung, S.; Garten, R.L. Strong metal-support interactions. Group 8 noble metals supported on titanium dioxide. *J. Am. Chem. Soc.* **1978**, *100*, 170–175. [[CrossRef](#)]
70. Tauster, S.; Fung, S.; Baker, R.; Horsley, J. Strong interactions in supported-metal catalysts. *Science* **1981**, *211*, 1121–1125. [[CrossRef](#)] [[PubMed](#)]
71. Lentz, C.; Jand, S.P.; Melke, J.; Roth, C.; Kaghazchi, P. DRIFTS study of CO adsorption on Pt nanoparticles supported by DFT calculations. *J. Mol. Catal. A Chem.* **2017**, *426*, 1–9. [[CrossRef](#)]
72. Martinelli, M.; Gnanamani, M.K.; LeViness, S.; Jacobs, G.; Shafer, W.D. An overview of Fischer-Tropsch Synthesis: XtL processes, catalysts and reactors. *Appl. Catal. A Gen.* **2020**, *608*, 117740. [[CrossRef](#)]
73. Fischer, N.; Van Steen, E.; Claeys, M. Preparation of supported nano-sized cobalt oxide and fcc cobalt crystallites. *Catal. Today* **2011**, *171*, 174–179. [[CrossRef](#)]
74. Kharisov, B.I.; Kharisova, O.V.; Ortiz-Mendez, U. *CRC Concise Encyclopedia of Nanotechnology*; CRC Press: Boca Raton, FL, USA, 2016.
75. Gholami, Z.; Tišler, Z.; Rubáš, V. Recent advances in Fischer-Tropsch synthesis using cobalt-based catalysts: A review on supports, promoters, and reactors. *Catal. Rev.* **2021**, *63*, 512–595. [[CrossRef](#)]
76. Liu, X.; Atwater, M.; Wang, J.; Huo, Q. Extinction coefficient of gold nanoparticles with different sizes and different capping ligands. *Colloids Surf. B* **2007**, *58*, 3–7. [[CrossRef](#)] [[PubMed](#)]

77. Prathibha, V.; Karthika, S.; Cyriac, J.; Sudarasanakumar, C.; Unnikrishnan, N. Synthesis of pure anatase TiO₂ nanocrystals in SiO₂ host and the determination of crystal planes by ImageJ. *Mater. Lett.* **2011**, *65*, 664–666. [[CrossRef](#)]
78. Biesinger, M.C.; Payne, B.P.; Grosvenor, A.P.; Lau, L.W.; Gerson, A.R.; Smart, R.S.C. Resolving surface chemical states in XPS analysis of first row transition metals, oxides and hydroxides: Cr, Mn, Fe, Co and Ni. *Appl. Surf. Sci.* **2011**, *257*, 2717–2730. [[CrossRef](#)]

Disclaimer/Publisher’s Note: The statements, opinions and data contained in all publications are solely those of the individual author(s) and contributor(s) and not of MDPI and/or the editor(s). MDPI and/or the editor(s) disclaim responsibility for any injury to people or property resulting from any ideas, methods, instructions or products referred to in the content.